JACS
JOURNAL OF THE AMERICAN CHEMICAL SOCIETY

Article

pubs.acs.org/JACS

Locating Organic Guests in Inorganic Host Materials from X-ray Powder Diffraction Data

Stef Smeets,[†,§] Lynne B. McCusker,[*,†] Christian Baerlocher,[†] Saleh Elomari,[‡] Dan Xie,[‡] and Stacey I. Zones[‡]

[†]Laboratory of Crystallography, ETH Zurich, Vladimir-Prelog-Weg 5, Zurich CH-8093, Switzerland

[‡]Chevron Energy Technology Company, Richmond, California 94802, United States

Supporting Information

ABSTRACT: Can the location of the organic structure-directing agent (SDA) inside the channel system of a zeolite be determined experimentally in a systematic manner? In an attempt to answer this question, we investigated six borosilicate zeolites of known framework structure (SSZ-53, SSZ-55, SSZ-56, SSZ-58, SSZ-59, and SSZ-60), where the location of the SDA had only been simulated using molecular modeling techniques in previous studies. From synchrotron powder diffraction data, we were able to retrieve reliable experimental positions for the SDA by using a combination of simulated annealing (global optimization) and Rietveld refinement. In this way, problems arising from data quality and only partially compatible framework and SDA symmetries, which can lead to indecipherable electron density maps, can be overcome. Rietveld refinement using geometric restraints were then performed to optimize the positions and conformations of the SDAs. With these improved models, it was possible to go on to determine the location of the B atoms in the framework structure. That is, two pieces of information that are key to the understanding of zeolite synthesis—the location of the organic SDA in the channel system and of the positions adopted by heteroatoms in the silicate framework—can be extracted from experimental data using a systematic strategy. In most cases, the locations of the SDAs determined experimentally compare well with those simulated with molecular modeling, but there are also some clear differences, and the reason for these differences can be understood. The approach is generally applicable, and has also been used to locate organic guests, linkers, and ligands in metal−organic compounds.

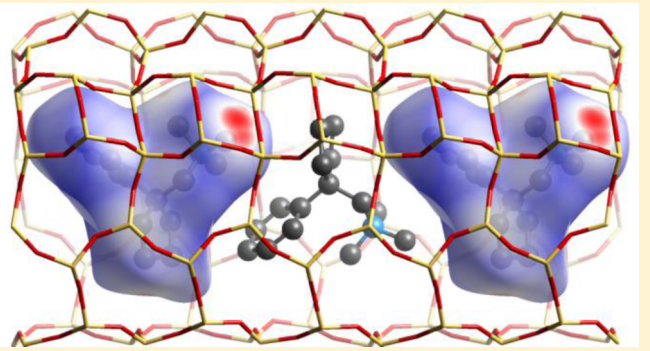

INTRODUCTION

It is well-known that the organic guest molecules introduced into a zeolite synthesis gel play a key role as structure-directing agents (SDA) and can have a profound effect on the micropore topology that results.[1] Several groups have performed large systematic studies on the effect of the charge, shape, size and composition of the SDA on the host−guest interaction.[2−5] Indeed, understanding the host−guest interaction of the SDA with the zeolite framework is crucial, if we are to understand why and how these materials form. This fact has fueled efforts to use and improve computational models to predict the host−guest interaction[6] and thereby direct the synthesis,[7] with the ultimate goal of using this information for the rational design of zeolites.[8]

It would be beneficial, therefore, if the locations of the organic guest species could also be retrieved experimentally, and X-ray diffraction methods would be ideal for this. Nowadays, it is generally accepted that framework structures can be solved using X-ray powder diffraction (XPD) data, and that the locations of inorganic cations can be found in difference electron density maps during the course of a Rietveld refinement. However, this is not yet the case for organic SDAs.

The key difficulty in locating organic guest species in inorganic host structures from diffraction data is that organic compounds consist of light scatterers and typically have low point symmetry, while their inorganic hosts consist of heavier scatterers and have high symmetry. These features result in a lack of contrast that makes it difficult to "see" the organic guest, and because of the difference in symmetry, the guest molecule often appears to be disordered. Even when decent quality single-crystal X-ray diffraction (XRD) data are available, these two factors alone make retrieving the location of the organic species challenging. The problem is exacerbated by the fact that many industrially and commercially important materials can only be produced in polycrystalline form, so conventional XRD analysis cannot be applied and XPD techniques are usually the only option. The process of locating the SDA using XPD data is often hindered by the quality of the data that can be collected. The problem may be low data resolution (no diffraction at higher angles or broad peaks), or in the assignment of reflection intensities due to reflection overlap, a problem that is

Received: March 24, 2016

DOI: 10.1021/jacs.6b02953
J. Am. Chem. Soc. XXXX, XXX, XXX−XXX

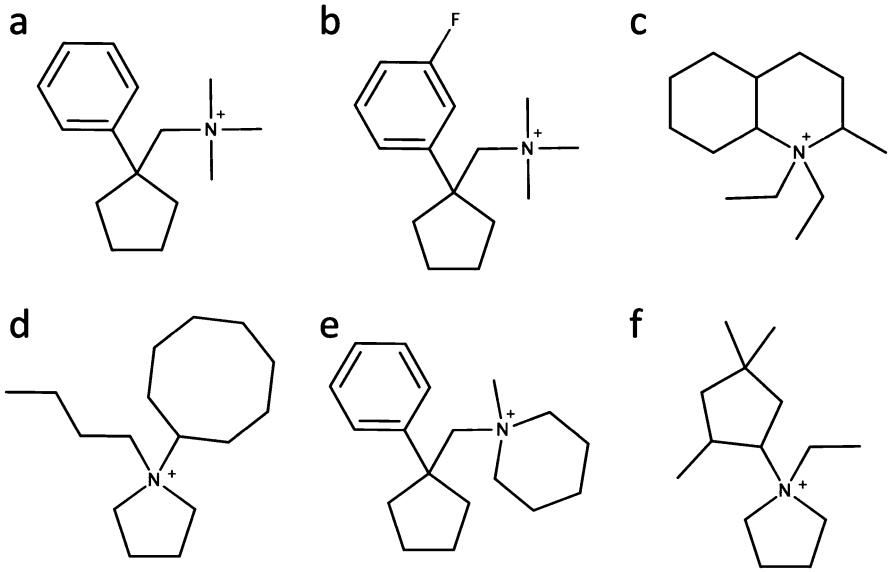

Figure 1. Schematic representation of the SDAs that were used in the syntheses of (a) SSZ-53: *N*,*N*,*N*-trimethyl-1-(1-phenylcyclopentyl)-methanaminium, (b) SSZ-55: 1-(1-(3-fluorophenyl)cyclopentyl)-*N*,*N*,*N*-trimethylmethanaminium, (c) SSZ-56: 1,1-diethyl-2-methyldecahydroquinolinium, (d) SSZ-58: 1-butyl-1-cyclooctylpyrrolidinium, (e) SSZ-59: 1-methyl-1-((1-phenylcyclopentyl)methyl)piperidinium, and (f) SSZ-60: 1-ethyl-1-(2,4,4-trimethylcyclopentyl)-pyrrolidinium.

ubiquitous in powder diffraction. This adds a second layer of complication that often results in the guest species simply being dismissed as "disordered".

Perhaps for these reasons, the location of the SDA in most studies is ignored, and structure analysis is performed using data collected on the calcined material. This is undesirable, because calcination typically leads to a reduction in the quality of the data that can be collected, and information about the synthesis is lost. In such cases, the location of the SDA is sometimes simulated using molecular dynamics modeling,[6] and this was the case for the samples that are the subject in this study. Our experience with zeolites, however, shows that these species are actually highly ordered, and their arrangements within the pores can often be described well by a superposition of discrete positions, provided the discrepancies in the symmetries can be resolved. With the limitations imposed by XPD data in mind, we have devised a systematic approach to determining the location of low-symmetry guest molecules in high-symmetry inorganic host materials using XPD data.

Summary of Previous Work. The first studies in which an organic SDA was found in a zeolite host surfaced in the late sixties–early seventies, when TMA was located in the cages of two synthetic zeolites using X-ray powder diffraction: in sodalite (**SOD**; cubic)[9] and in Na–P1 (**GIS**; tetragonal).[10,11] In the same period, the pentagondodecahedral arrangement of water molecules in the sodium aluminosilicate zeolite A was reported.[12] Later, the location of the tetrapropyl ammonium (TPA) cation in the channel system of ZSM-5 was achieved, first using single-crystal XRD data,[13,14] and later using XPD data.[15] This served as an important model system for studying guest–host relationships in molecular sieves, because it provided detailed coordinates against which theoretical molecular modeling techniques could be validated.[16]

An experimental determination of the location of the organic guest molecules is generally performed by careful analysis of difference electron density maps, e.g., refs 17–19. By assigning atoms to the electron density one-by-one, it is possible to build the SDA to determine its location in the pores. This procedure is typically reserved for cases where single-crystal, or high quality XPD data are available, and disorder is low. Others have taken a more pragmatic approach, and rely on molecular modeling to find an initial location for the SDA, and used this as a starting point for the Rietveld refinement.[20–22]

Using Simulated Annealing. Simulated annealing is a global optimization routine that is part of the direct-space class of methods for crystal structure determination.[23] Such methods are already implemented in a large number of crystallographic program suites, and work especially well when some a priori information about the system, such as chemical composition, geometry, and/or connectivity, is known. It is particularly well-suited for organic and pharmaceutical compounds, where such information is usually available. Expected atoms, molecules or fragments are placed randomly in the unit cell as rigid bodies and then moved around by modifying their positions, orientations and free torsion angles using the simulated annealing algorithm. After each rearrangement, the difference between the experimental and calculated profile is evaluated, and the cycle is repeated until convergence has been reached. This process is repeated until a satisfactory model that fits the data emerges.

Typically, the determination of a zeolite structure is split into two parts: (1) determining the framework structure, and (2) locating extra-framework species in the pores. Although simulated annealing has been used in a few instances to determine the framework structure of a zeolite, for example UiO-6 (**OSI**)[24] and ERS-7 (**ESV**),[25] this step is usually performed using other techniques.[26] The chemical composition and connectivity of the organic guest is generally known, and can be confirmed using elemental analysis and solid state ^{13}C NMR, respectively. In other words, a significant amount of useful a priori information is available. The simulated annealing routine is therefore ideally suited to locating the organic species in the pores. Because the algorithm uses the experimental diffraction pattern directly, the data quality is reflected in the profile parameters used to calculate the pattern for each model it generates. Furthermore, complicated partial occupancies

DOI: 10.1021/jacs.6b02953
J. Am. Chem. Soc. XXXX, XXX, XXX–XXX

arising from the SDA being on or near a high-symmetry position are taken into account automatically.

This approach to locating the organic SDA in zeolites was developed during the course of the structure analyses of SSZ-45,[27] SSZ-61,[28] SSZ-87,[29] and Ge-**BEC**.[30] In SSZ-45, the SDA was initially found by simulated annealing at a position with mirror (2-fold) symmetry. During the refinement of the atomic positions, the SDA seemed to align itself along the mirror plane of the framework on a position with 2-fold disorder. By fixing the mirror plane present in the SDA to the one of the framework, the disorder in the SDA could be resolved. The case of SSZ-87 was similar. There, the SDA was found at a position of $2/m$ (4-fold) symmetry, but the rotation axis of the SDA could be aligned with that of the framework, and this resulted into two highly ordered, though overlapping, positions for the SDA. SSZ-61 and Ge-**BEC** are two examples where the location of the SDA could be determined despite the low quality of the data. We have also used the method to locate indigo sorbed in silicalite-1,[31] and other researchers have used variations of this method to locate sorbed guest molecules in zeolites.[32−34]

Although our main focus here is on the structure analysis of zeolites, the method is quite general for locating organic guest species in inorganic host materials. We have applied it to locate the organic species between the zirconium phosphate layers of ZrPOF-EPY,[35] the ligand in a Mo oxide/pyrazolylpyridine polymeric hybrid material,[36] and the ligand of a Cu coordination complex that was part of a multiphase product obtained by decomposing the metal−organic framework of HKUST-1.[37] In the case of ZIF-L,[38] we were only able to locate the Zn anions initially, and used simulated annealing to simplify the problem of locating the organic linker.

Aim of This Study. As the simulated annealing routine had proven to be useful in locating organic guest molecules in a reasonable number of zeolites and to be flexible enough to deal with other types of inorganic materials also, we were interested to see whether it could be applied in systematic manner. For this purpose, samples of the borosilicates SSZ-53 (**SFH**),[39] SSZ-55 (**ATS**),[40,41] SSZ-56 (**SFS**),[42] SSZ-58 (**SFG**),[43] SSZ-59 (**SFN**),[39] and SSZ-60 (**SSY**),[44] which were produced using the SDAs shown in Figure 1, were investigated. These were selected because (1) they are prepared with bulky and flexible SDAs, which are challenging to locate, (2) they provide a series with closely related SDAs and frameworks, and (3) the location of the SDA was originally simulated using molecular dynamics modeling. The idea behind the latter was that the results might provide some insight into the reliability of simulated SDA locations.

EXPERIMENTAL SECTION

Synthesis. Samples of the borosilicate zeolites SSZ-53, SSZ-55, SSZ-56, SSZ-58, SSZ-59, and SSZ-60 were prepared as described in the literature.[39,40,42−44]

X-ray Powder Diffraction Data Collection. Synchrotron XPD data were collected on as-synthesized samples of the borosilicates SSZ-53, SSZ-55, SSZ-56, SSZ-58, SSZ-59, and SSZ-60 in 0.3 mm capillaries at a wavelength of 0.7749 Å with a Mythen II detector on the MS-Powder beamline at the Swiss Light Source in Villigen, Switzerland.[45]

Methods. The procedure described here can be started once the framework structure is known, and assumes that the chemical composition of the organic guest is known a priori. It is usually a good idea to perform an optimization of the zeolite geometry, e.g., by using a distance-least-squares refinement[46] or performing a "penalties only" refinement against the restraints using a program like TOPAS,[47] and to initiate the structure completion using this model. The reflection intensities in the low 2θ angle range are most affected by the position of the SDA, so a reliable estimate for the scale factor can be obtained by refining it against the high-angle data only. A difference electron density map using the whole data set should then reveal electron density inside the channel system corresponding to the position of the SDA or any other extra-framework atoms or heteroatoms (e.g., Figure 2). Such maps can be visualized using programs like VESTA[48] or Chimera,[49] and offer a low resolution visualization of the SDA.

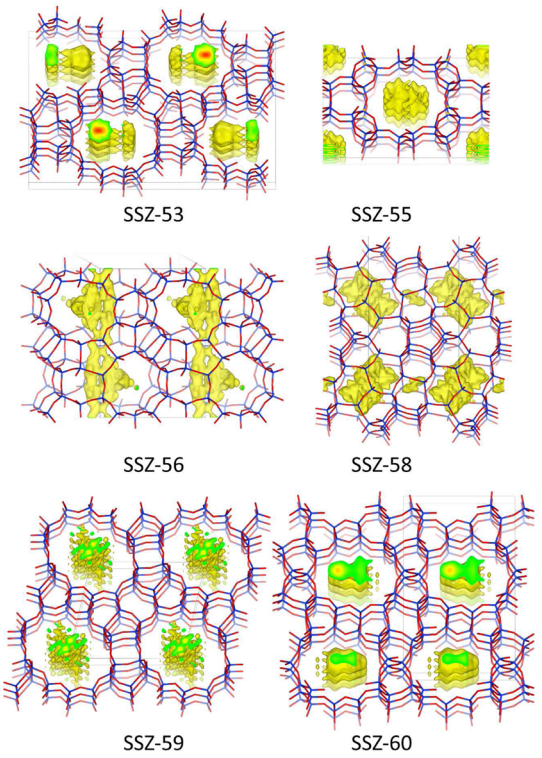

Figure 2. Difference electron density maps of SSZ-53 (along *a*), SSZ-55 (along *c*), SSZ-56 (along *c*), SSZ-58 (along *b*), SSZ-59 (along *a*), and SSZ-60 (along *c*) after initial scaling, showing the positive differences only. For SSZ-53, SSZ-55, SSZ59, and SSZ-60, three unit cells stacked along the channel direction are shown. The surface of the electron clouds is shown in yellow. Where the electron density is cut (i.e., at the cell edges), the color gradient (green to red) corresponds to increasing electron density. Images were generated using VESTA.[48]

If the 3-dimensional structure of the organic guest is not known from a separate XRD experiment or the Cambridge structural database (CSD),[50] it can be generated and optimized using the energy minimization routine in a program like Jmol[51] or Avogadro.[52] It is then introduced into the simulated annealing program as a rigid-body model, fixing all parameters other than those describing the rotation/translation of the SDA(s). A detailed description of the method (including examples) has been provided in the Supporting Information.

RESULTS

The procedure described above was applied to each of the measured data sets. Structure refinements were initiated using the published framework coordinates (Table 1), and the initial difference electron density maps after scaling are shown in Figure 2. Crystallographic details for each material, and their structure refinements (including profile plots), can be found in the Supporting Information. The samples can be divided in two groups: (a) those with one-dimensional (SSZ-53, SSZ-55, SSZ-59, SSZ-60) and those with two-dimensional channel systems

DOI: 10.1021/jacs.6b02953
J. Am. Chem. Soc. XXXX, XXX, XXX−XXX

Table 1. Published Lattice Parameters of the Six Zeolite Samples

	space group	a (Å)	b (Å)	c (Å)	α (deg)	β (deg)	γ (deg)
SSZ-53	$C2/c$	5.0192	33.7437	21.1653		90.49	
SSZ-55	$Cmc2_1$	12.9532	21.8510	5.0784			
SSZ-56	$P2_1/m$	13.9483	19.8958	12.3613		106.68	
SSZ-58	$Pmma$	25.1106	12.4972	12.8596			
SSZ-59	$P\bar{1}$	5.0231	12.7351	14.7219	103.44	90.51	100.88
SSZ-60	$P2_1nm$	21.9510	13.6985	5.0122			

(SSZ-56, SSZ-58). Because the latter are the more straightforward, they are discussed first.

Two-Dimensional Channel Systems. *SSZ-56.* The initial difference map for SSZ-56, generated in the space group $P2_1/m$, reveals residual electron density in the 12-ring channels running along the y-direction. The SDA is fairly rigid and lies in a 2-dimensional channel system. Both factors simplify the procedure for locating it. With the simulated annealing routine, the optimum position of the rigid-body model of the SDA could be found easily on a site with 2-fold symmetry (Figure 3).

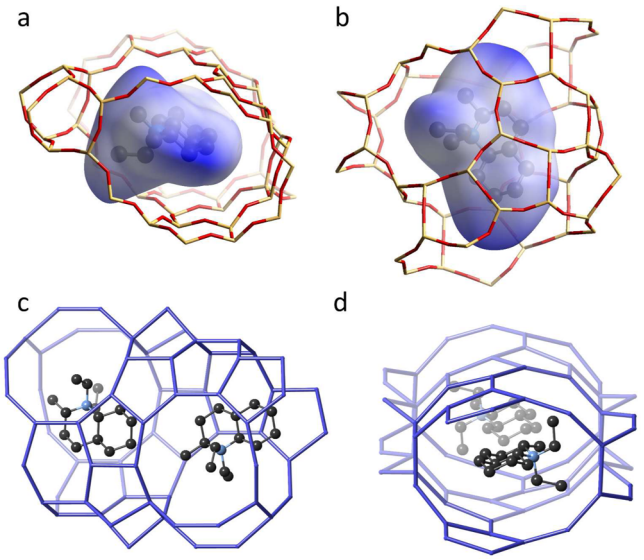

Figure 3. Views along (a) b and (b) c showing the Hirshfeld surface of the SDA and its location at the intersection of the pores of as-synthesized SSZ-56. Alternative views along (c) c and (d) b with framework O atoms omitted for clarity, show the packing of the SDA species.

Its occupancy refined to the expected value of 0.50, indicating that the space was fully occupied, so it was fixed at that value. There appeared to be large voids in the 10-ring channels running along z, with dimensions similar to those of the SDA, so the simulated annealing process was repeated with a second, crystallographically independent SDA included. However, this model did not converge. It was readily apparent that an SDA in this location would result in unacceptably short intermolecular contacts, and a poor fit to the data, so the second SDA was removed.

For these data, the fit improved significantly when a model for anisotropic line broadening[53] was applied. After a few cycles of Rietveld refinement, the rigid-body model for the SDA could be relaxed to one with geometric restraints. Once the SDA had been refined, the Si atoms in the framework were redefined as mixed Si/B sites, with a total occupancy of 1.0. Only two of the 14 sites showed significant B occupancy yielding a total of 0.88 B atoms per 56 T atoms (tetrahedrally coordinated atoms) in the unit cell (Si:B = 62.6:1). The refinement resulted in an excellent fit to the data (Figure S3) with agreement values R_I = 0.053 and R_{wp} = 0.103 (R_{exp} = 0.014). All intermolecular distances between the SDA and the framework O atoms are well above 3.4 Å (Table S3), indicating a very comfortable fit of the SDA to the host framework.

SSZ-58. The electron density in the difference map for SSZ-58 (Figure 2) shows the location of the SDA in the center of the intersection between the 12-ring channels on a site with 4-fold multiplicity. As with SSZ-56, a starting location for the SDA could be retrieved easily with the simulated annealing algorithm. The occupancy of the SDA refined to the expected value of 0.25 and was fixed at that value. In a subsequent difference map, there appeared to be some residual electron density in the channel along y, between the SDAs. There is not enough space for another (partially occupied) SDA, so a disordered water molecule with an occupancy of 0.25 was assigned to this position. This made a small, but noticeable difference to the profile fit. Again, the fit could be further improved by applying a model to describe the anisotropic line broadening.[53] The rigid-body model of the SDA was converted to a restrained one, but this appeared to distort the cyclo-octyl group of the SDA somewhat. A quick search of the CSD[50] revealed that several such 8-rings distorted in a similar manner, so the restrained model was retained (Figure 4). In this structure, the B occupancy was found to be significant at sites T2 (0.083 B, 0.917 Si), T7 (0.094 B, 0.906 Si), and T8 (0.058 B, 0.942 Si), giving a total of 1.88 B atoms per 74 T atoms in

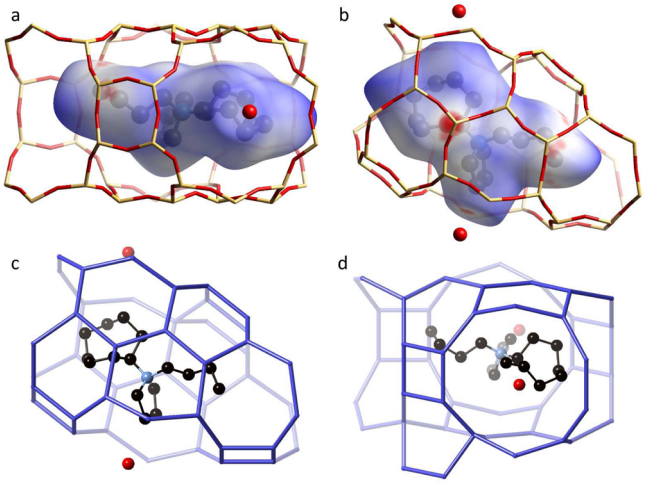

Figure 4. Views along (a) c and (b) b showing the Hirshfeld surface of the SDA and its location at the intersection of the pores of as-synthesized SSZ-58. Alternative views along (c) b and (d) c with framework O atoms omitted for clarity, show the packing of the SDA and the water molecules (red balls).

DOI: 10.1021/jacs.6b02953
J. Am. Chem. Soc. XXXX, XXX, XXX−XXX

the unit cell (Si:B 38.4:1). The refinement converged with agreement values R_I = 0.066 and R_{wp} = 0.115 (R_{exp} = 0.011), and a good fit to the data (Figure S4).

One-Dimensional Channel Systems. Unlike the samples described above, SSZ-53, SSZ-55, SSZ-59, and SSZ-60 have one-dimensional channel systems, and this complicates the procedure for locating the SDA. In addition to the expected disorder of the SDA arising from its being on a site of high symmetry, the crystallographic axes (*a* or *c*) in the channel direction are very short (ca. 5.0 Å), making it impossible for the SDA to fit in a single unit cell. In their study of SSZ-55 using single-crystal X-ray diffraction, Burton et al. described this as a lack of register in the location of the SDA between one zeolite channel and the next that results in a second source of disorder.[41]

The difference maps for each of these samples reveal continuous electron density that zigzags along the one-dimensional channel. Although it was possible to run the simulated annealing routine to get a location for the SDAs, the two sources of disorder resulted in 8 or more SDAs overlapping. This made visualization difficult, and resulted in a situation where almost any location of the SDA yielded a good fit to the data, but did allow us to estimate the population of the SDA.

SSZ-53. For SSZ-53, the SDA was located on a site with 2-fold symmetry, and its occupancy refined to 0.33 (i.e., 0.66 SDA molecules per channel per unit cell). In other words, there are approximately two SDAs per three unit cells, corresponding to the findings of Burton et al.,[39] who based their simulations on results from chemical analysis.

Therefore, a supercell was constructed by stacking three unit cells of SSZ-53 (omitting the SDA) along the *x*-direction. Initially, this operation was performed in symmetry *P*1, but the *ADDSYM* routine in *PLATON*[54] indicated that the framework symmetry of the supercell was $P2_1/c$, with 144 framework atoms in the asymmetric unit. A difference map with this supercell was similar to the one found originally. The simulated annealing routine was applied once again, this time with two independent molecules. With the reduction in symmetry, the SDAs are no longer disordered, and organize themselves along a 2_1 screw axis along the channel direction in an arrangement that is very similar to the results of the molecular modeling. To finalize the refinement at this stage, the rigid-body model of the SDA was converted to a restrained one, and both the framework and SDA were refined in the supercell (Figure 5). This resulted in a good fit to the data (R_{wp} = 0.118).

Then, from the refined positions of the SDAs in the supercell, the equivalent positions in the conventional cell (with the original Si atoms) were generated. This necessarily resulted in disordered, overlapping SDAs, but the restraints could be retained and the positions understood. The occupancies refined to approximately 1/6, so they were fixed at that value for the remainder of the refinement. Although the SDAs overlapped severely, their coordinates did not deviate much from their original values, meaning that the orientations found with the supercell were representative. The occupancies of the Si atoms were refined, and only those of Si3 and Si8 refined to values significantly lower than 1.0, so these were redefined as mixed Si/B sites. Their occupancies refined to 0.85 Si (0.15 B) and 0.89 Si (0.11 B), respectively, to give a total 2.5 B atoms per 64 T atoms in the unit cell (Si:B 25.7:1). The antibump function was applied between C and framework O atoms in the final stages of the refinement to maintain reasonable intermolecular

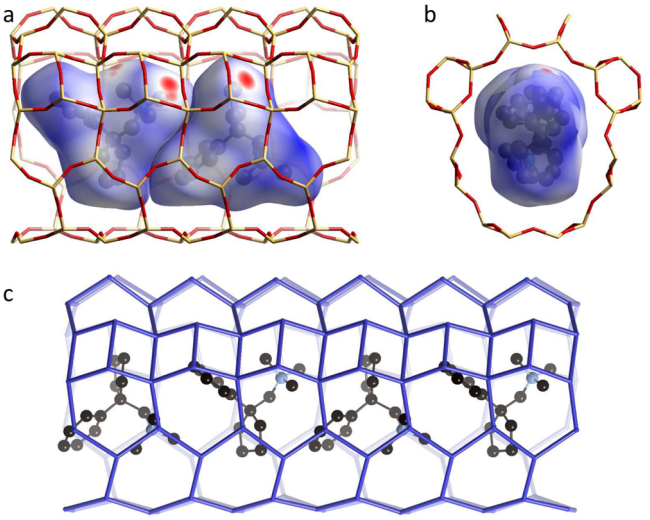

Figure 5. Views along (a) *c* and (b) *a* showing the location of the SDA and its Hirshfeld surface in the one-dimensional channel of as-synthesized SSZ-53. Alternative view along (c) *c*, with framework O atoms omitted for clarity, shows the SDA packing arrangement.

distances of over 3.0 Å. The final refinement resulted in an excellent fit to the data (Figure S1) with agreement values of R_I = 0.036 and R_{wp} = 0.088 (R_{exp} = 0.019).

SSZ-55 and SSZ-59. For SSZ-55 and SSZ-59, the procedure for locating the SDAs was similar to that used for SSZ-53. SSZ-55 required a supercell (space group *Cc*) consisting of three conventional cells stacked along the *z*-direction. The SDA could be found in an arrangement similar to that of SSZ-53 (Figure 6), giving us confidence that it was a reasonable

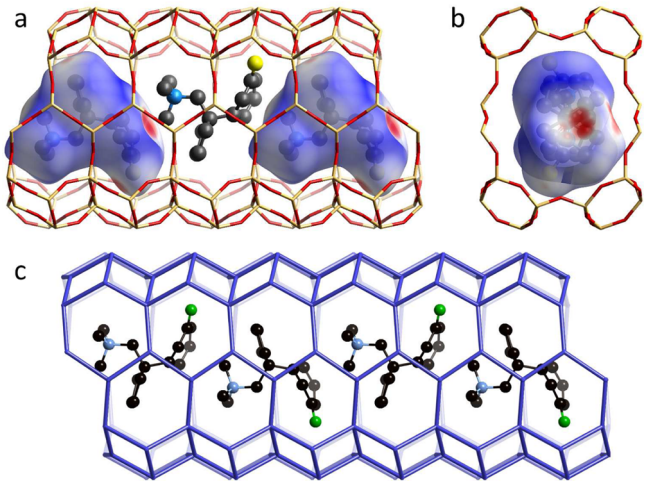

Figure 6. Views along (a) *a* and (b) *b* showing the location of the SDA and its Hirshfeld surface in the one-dimensional channel of as-synthesized SSZ-55. Alternative view along (c) *a*, with framework O atoms omitted for clarity, shows the SDA packing arrangement.

solution. Rietveld refinement of the framework and SDA was performed in $C222_1$, taking the position of the SDA from the supercell. Further refinement showed that B atoms occupy the T1 position preferentially (0.86 Si, 0.14 B), giving rise to a total 1.12 B atoms per 24 T atoms in the unit cell (Si:B 20.4:1). The occupancy of the SDA refined to 0.130, which is lower than the 1/6 that would correspond to maximum loading. The final refinement resulted in a good fit to the data (Figure S2) with

DOI: 10.1021/jacs.6b02953
J. Am. Chem. Soc. XXXX, XXX, XXX−XXX

agreement values R_I = 0.078 and R_{wp} = 0.150 (R_{exp} = 0.010). The major differences are in the peak shapes, which were difficult to model. The shortest intermolecular distances between the SDA and the framework are 2.926(3) Å, 2.974(3) Å, 2.975(4) Å, 2.979(4) Å, and 2.995(3) Å, which are lower than for the other zeolites. This indicates a relatively tight fit of the SDA within the framework. All other distances are over 3.0 Å.

For SSZ-59, the SDA was located using a supercell (space group $P\bar{1}$) consisting of three conventional cells stacked along the *x*-axis. The SDAs were arranged in alternating fashion, so that either the piperidinium or the benzyl ring of neighboring molecules face one another (Figure 7). Initially, some of the

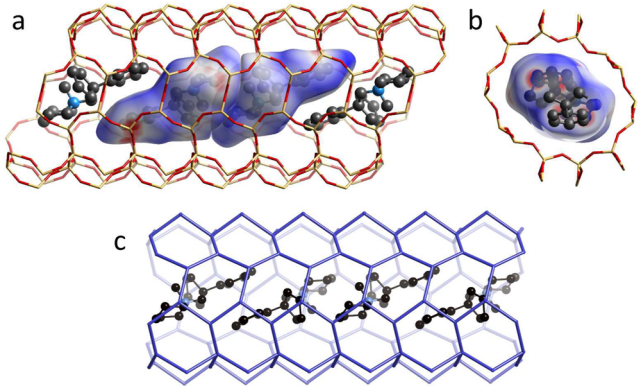

Figure 7. Views along (a) *c* and (b) *a* showing the location of the SDA and its Hirshfeld surface in the one-dimensional channel of as-synthesized SSZ-59. Alternative view along (c) *c*, with framework O atoms omitted for clarity shows the SDA packing arrangement.

intermolecular distances were on the low side (down to 2.6 Å), but by slowly increasing the value of the antibump function from 2.6 to 3.1 Å, these distances could be improved. At this point, the rigid-body model for the SDA was converted to a restrained one, and a model for anisotropic line broadening was applied.[53] While the refinement converged, significant positive differences were observed for the three strong low-angle reflections. Only by refining the occupancy of the SDA could these differences be removed. It appears that the situation in SSZ-59 is similar to that of SSZ-55, as the occupancy of the SDA refined to approximately 0.80. Structure refinement in the supercell resulted in a good fit to the data. The coordinates of the SDA in the supercell were transformed to those in the conventional one, and refinement was performed in space group $P\bar{1}$. After the refinement converged, a good fit to the data was obtained (Figure S5) with agreement values R_I = 0.036 and R_{wp} = 0.088 (R_{exp} = 0.019). B is preferentially located on T6 (0.87 Si, 0.13 B) and T7 (0.94 Si, 0.06 B) to give a total occupancy of 0.38 B per 16 T atoms in the unit cell (Si:B 41.1:1). The shortest intermolecular distances between the SDA and the framework are 3.062(4) Å, 3.076(3) Å, 3.077(2) Å, and 3.079(3) Å. All other distances are over 3.1 Å.

SSZ-60. The data collected in SSZ-60 (Figure S6) are noticeably worse than those obtained for the other materials. They are also poorer than those reported previously.[44] The peaks are broader, the noise level is higher, and the signal dies out at lower 2θ angle. Despite this, a difference electron density map clearly reveals electron density inside the one-dimensional channel system (Figure 2). However, it proved to be difficult to find a stable position for the SDA that both fits the data and makes chemical sense. Therefore, in view of the poor quality of the data, and the fact that the one-dimensional channel system adds a second layer of disorder, further study of SSZ-60 was abandoned.

DISCUSSION

It is often said that the SDA has a space-filling role in the formation of zeolite frameworks. This is well-illustrated by the Hirshfeld surfaces for the structures described here (Figures 3–7). The color scheme used on this surface indicates the contact distance to the framework. Where the contacts are about equal to the sum of the van der Waals radii, the surface is colored white, short contacts are highlighted in red, and long ones in blue. In each of the examples presented here, the framework wraps neatly around the SDA with a minimum $C_{SDA}\cdots O_{framework}$ distance of 3.0 to 3.5 Å (Table S3).

However, there is more to the location of the SDA than just a nice fit to the pore. Our findings show that the SDA is usually highly ordered, and only adopts a handful of locations within the pores and these are related by symmetry. This means that the chemical surroundings for each SDA are virtually identical. Because of this, it is sometimes possible to relate the location of the SDA to the structural features in the framework directly. This is especially noticeable in the zeolites with one-dimensional channel systems (SSZ-53, SSZ-55, SSZ-59, and SSZ-61), where the bulky part of the SDA is perfectly aligned with the corrugations of the channels.

The location of the B atoms in these borosilicates can also be influenced by the location of the N^+ in the SDA. We have seen this previously in SSZ-87, where the B atoms occupy the two crystallographically independent T positions that are in closest proximity to the N^+ of the SDA. For SSZ-53 and SSZ-55, where the N^+ in the SDA is also relatively exposed, the B atoms occupy the T positions closest to these N^+ centers. Furthermore, in SSZ-55, the F atom in the SDA approaches the center of the 6-ring formed by 4 Si1 (partially occupied by B) and 2 Si3, at a distance of 3.2 to 3.5 Å from Si1. For SSZ-56, SSZ-58, and SSZ-59, the N^+ is part of a cyclic group and less exposed than in the previous examples. Although in these three structures the B atoms are along the channel walls, they are not in the positions closest to the N atoms of the SDAs, and there appears to be no structural relationship between the location of B and N in these cases.

On the basis of our experience in using simulated annealing to locate SDAs with XPD data, we can identify two situations in zeolites. If the SDA is trapped, for example when it is in a cage (SSZ-45, SSZ-87) or at a channel intersection (SSZ-56, SSZ-58, SSZ-61, ZSM-5), its location is well-defined and translational symmetry is preserved. This facilitates the global optimization, and makes locating a starting position for refinement straightforward. For these cases, the results presented in this study, show that a systematic approach to the location of the SDA with XPD data is indeed possible.

In the other situation, when the SDA is in a one-dimensional channel (SSZ-53, SSZ-55, SSZ-59, SSZ-60), the translational symmetry is lost. That is, the SDA can only adopt an ordered arrangement within each channel if the unit cell is expanded along the channel direction. Unfortunately, the arrangements in the different channels are not in register with one another, so the resulting difference maps show a continuous cloud of electron density that is difficult to interpret. The approach presented here can still be applied, but involves an extra step to generate the appropriate supercell, so that a model in which the

DOI: 10.1021/jacs.6b02953
J. Am. Chem. Soc. XXXX, XXX, XXX–XXX

SDA is fully ordered can be constructed. It should be noted here that there is no evidence in the data for this supercell, but that it is necessary as an intermediate step to find a suitable starting location for the SDA. One of the assumptions here is that the framework pores of as-synthesized zeolites are fully loaded. However, SSZ-55 and SSZ-59 showed a maximum occupancy of 0.8 SDAs per channel per unit cell, and this introduces an ambiguity in the analysis. This could simply be interpreted that there is no need for a full occupancy of the SDA to ensure successful growth of this and only this structure type. Nonetheless, our refinements show that by using a supercell to perform simulated annealing, it is possible to obtain a chemically sensible model in a systematic manner. In all cases, independent measurements, such as ^{13}C NMR or CHN elemental analysis are recommended to confirm that the SDA is intact and included in the structure.

Comparison with Molecular Modeling. For SSZ-56, we find a good agreement between the location of the SDA with molecular modeling simulations and our XPD study (Figure S7). Although our model has two crystallographically equivalent positions for the SDA, one of the possible arrangements is essentially identical to the one found with molecular modeling. We reason that in this case the rigidity of the SDA, the fact that N^+ is relatively well shielded, and the fact that the fit of the SDA in the framework is not tight are helpful factors for successful molecular modeling simulations. For SSZ-58, on the other hand, there is a clear difference between the experimental and theoretical result, because the model used in the latter was incomplete. The presence of water was not taken into account, and this leads to a different outcome (Figure S8).

Of the four zeolites with one-dimensional channel systems, our results for SSZ-53 and SSZ-55 compare reasonably well with those obtained previously using molecular modeling (Figure S9). Both approaches reveal similar pairwise arrangements of the SDAs. The bulky parts of the SDAs follow the corrugations of the one-dimensional channel. On the basis of the total electron content of the SDA in the channels, we were able to estimate the occupancy of the SDAs per channel per cell to be 2/3. This interpretation matches that of Burton et al.,[39,41] who also found that a supercell consisting of three conventional cells stacked along the channel direction should be constructed to accommodate two SDA molecules in an optimal fashion.

Only for SSZ-59, does our interpretation significantly deviate from the one reported by Burton et al.,[39] who found that the unit cell should be quadrupled (rather than tripled) to allow for the optimal arrangement of the SDA. There was no indication from the XPD data alone that indicated that a quadrupling (or indeed tripling) of the unit cell was necessary. An attempt was made to find a position of the SDA using a supercell consisting of two conventional cells, which is also in line with the number of SDAs per channel per conventional cell (1/2) found by Burton et al. In this way, it was possible to find a geometrically reasonable position for the SDA in the center of the channel, but its occupancy refined to 0.65, which means that SDAs from neighboring unit cells overlap. Therefore, it appears that in this case the refined structure from the XPD data with two SDAs per three unit cells is more likely.

CONCLUSION

Our analyses demonstrate that the SDA can be located systematically using XPD methods. The difficulty in finding a starting location for the SDA depends on the problem at hand. In the case of a rigid SDA or a well-defined channel system (SSZ-56, SSZ-58), locating the SDA from XPD data can be straightforward. More difficult cases like those of SSZ-53, SSZ-55, and SSZ-59 require that an appropriate supercell be constructed, but then the same systematic approach can be applied. For SSZ-60 it was not possible to find a chemically sensible position for the SDA from the poor data, but even in this case, the difference map shows corrugations similar to those obtained for SSZ-53, SSZ-55, and SSZ-59, which may give at least partial information about the location of the SDA in that material.

We have now examined a number of as-synthesized zeolites, and find that the SDA is generally well ordered. It just does not have the full symmetry of the framework structure and therefore appears to be disordered. Comparison with the results from molecular modeling is mixed. In some cases (SSZ-53, SSZ-55, SSZ-56), there is a good agreement between the two methods, but in others (SSZ-58, SSZ-59), there are some clear differences. The latter emanate from the fact that the models used for the simulations did not include the positions of the B atoms or (in the case of SSZ-58) H_2O in the model. Simulations including this additional information could lead to more similar results, and indeed combining the two methods could be quite powerful.

Although our main interest is in zeolites, simulated annealing is a generally applicable tool that is ideal for structure completion problems. As such, it can also be used to locate organic molecules, such as linkers, ligands, and SDAs in metal–organic species. The fact that experimental and computational techniques have advanced to a level that organic species can be located systematically has important implications for understanding the synthesis procedure,[55] and may offer new insight into host–guest interactions that play a crucial role in the formation of such materials.

ASSOCIATED CONTENT

Supporting Information

The Supporting Information is available free of charge on the ACS Publications website at DOI: 10.1021/jacs.6b02953.

Detailed description of the method, detailed information on the structure analyses of as-synthesized SSZ-53, SSZ-55, SSZ-56, SSZ-58, SSZ-59, and SSZ-60, including Rietveld plots, selected bond distances, and crystallographic data of the refined structures and corresponding idealized models (for visualization only). (PDF)
Crystal data of as-synthesized SSZ-53 (CIF)
Crystal data of as-synthesized SSZ-55 (CIF)
Crystal data of as-synthesized SSZ-56 (CIF)
Crystal data of as-synthesized SSZ-58 (CIF)
Crystal data of as-synthesized SSZ-59 (CIF)
Idealized model of as-synthesized SSZ-53 (CIF)
Idealized model of as-synthesized SSZ-55 (CIF)
Idealized model of as-synthesized SSZ-56 (CIF)
Idealized model of as-synthesized SSZ-58 (CIF)
Idealized model of as-synthesized SSZ-59 (CIF)

AUTHOR INFORMATION

Corresponding Author

*mccusker@mat.ethz.ch

Present Address

[§]Department of Material and Environmental Chemistry, University of Stockholm, Svante Arrhenius väg 16C, SE-106 91 Stockholm, Sweden.

DOI: 10.1021/jacs.6b02953
J. Am. Chem. Soc. XXXX, XXX, XXX–XXX

Notes

The authors declare no competing financial interest.

■ ACKNOWLEDGMENTS

We thank Antonio Cervellino for his assistance with the powder diffraction measurements on the Materials Science Beamline at the SLS in Villigen, Switzerland. This work was supported by the Swiss National Science Foundation and the Chevron Energy Technology Company.

■ REFERENCES

(1) Lobo, R. F.; Zones, S. I.; Davis, M. E. *J. Incl. Phenom. Macrocycl. Chem.* **1995**, *21* (1−4), 47−78.
(2) Gies, H.; Marler, B. *Zeolites* **1992**, *12* (1), 42−49.
(3) Gies, H. In *Advanced Zeolite Science and Applications*; Jansen, J. C., Karge, H. G., Weitkamp, J., Eds.; Elsevier, 1994; Vol. *85*, pp 295−327.
(4) Kubota, Y.; Helmkamp, M. M.; Zones, S. I.; Davis, M. E. *Microporous Mater.* **1996**, *6* (4), 213−229.
(5) Wagner, P.; Nakagawa, Y.; Lee, G. S.; Davis, M. E.; Elomari, S.; Medrud, R. C.; Zones, S. I. *J. Am. Chem. Soc.* **2000**, *122* (2), 263−273.
(6) Burton, A.; Lee, G. S.; Zones, S. I. *Microporous Mesoporous Mater.* **2006**, *90* (1−3), 129−144.
(7) Pulido, A.; Moliner, M.; Corma, A. *J. Phys. Chem. C* **2015**, *119* (14), 7711−7720.
(8) Yu, Y.; Xu, R. *Acc. Chem. Res.* **2010**, *43* (9), 1195−1204.
(9) Baerlocher, C.; Meier, W. M. *Helv. Chim. Acta* **1969**, *52* (7), 1853−1860.
(10) Baerlocher, C.; Meier, W. M. *Helv. Chim. Acta* **1970**, *53* (6), 1285−1293.
(11) Baerlocher, C.; Meier, W. M. *Z. Kristallogr.* **1972**, *135*, 339−354.
(12) Gramlich, V.; Meier, W. M. *Z. Kristallogr.* **1971**, *133* (1−6), 134−149.
(13) Price, G. D.; Pluth, J. J.; Smith, J. V.; Araki, T.; Bennett, J. M. *Nature* **1981**, *292* (5826), 818−819.
(14) Price, G. D.; Pluth, J. J.; Smith, J. V.; Bennett, J. M.; Patton, R. L. *J. Am. Chem. Soc.* **1982**, *104* (22), 5971−5977.
(15) Baerlocher, C. In *6th Int. Zeolite Conf.*; Olson, D. H., Bisio, A., Eds.; Guildford Butterworths: Reno, 1984; pp 823−833.
(16) Catlow, R.; Bell, R.; Cora, F.; Slater, B.; Cejka, J.; van Bekkum, H.; Corma, A.; Schüth, F. *Stud. Surf. Sci. Catal.* **2007**, *168*, 659−700.
(17) Jordá, J. L.; McCusker, L. B.; Baerlocher, C.; Morais, C. M.; Rocha, J.; Fernandez, C.; Borges, C.; Lourenco, J. P.; Ribeiro, M. F.; Gabelica, Z. *Microporous Mesoporous Mater.* **2003**, *65* (1), 43−57.
(18) Camblor, M. A.; Díaz-Cabañas, M.-J.; Perez-Pariente, J.; Teat, S. J.; Clegg, W.; Shannon, I. J.; Lightfoot, P.; Wright, P. A.; Morris, R. E. *Angew. Chem., Int. Ed.* **1998**, *37* (15), 2122−2126.
(19) Zanardi, S.; Alberti, A.; Cruciani, G.; Corma, A.; Fornés, V.; Brunelli, M. *Angew. Chem., Int. Ed.* **2004**, *43* (37), 4933−4937.
(20) Yang, X.; Camblor, M. A.; Lee, Y.; Liu, H.; Olson, D. H. *J. Am. Chem. Soc.* **2004**, *126* (33), 10403−10409.
(21) Baerlocher, C.; Xie, D.; McCusker, L. B.; Hwang, S.-J.; Chan, I. Y.; Ong, K.; Burton, A. W.; Zones, S. I. *Nat. Mater.* **2008**, *7* (8), 631−635.
(22) Xie, D.; McCusker, L. B.; Baerlocher, C.; Zones, S. I.; Wan, W.; Zou, X. *J. Am. Chem. Soc.* **2013**, *135* (28), 10519−10524.
(23) David, W. I. F.; Shankland, K. *Acta Crystallogr., Sect. A: Found. Crystallogr.* **2008**, *64* (1), 52−64.
(24) Akporiaye, D. E.; Fjellvag, H.; Halvorsen, E. N.; Haug, T.; Karlsson, A.; Lillerud, K. P. *Chem. Commun.* **1996**, No. 13, 1553−1554.
(25) Campbell, B. J.; Cheetham, A. K.; Bellussi, G.; Carluccio, L.; Perego, G.; Millini, R.; Cox, D. E. *Chem. Commun.* **1998**, No. 16, 1725−1726.
(26) McCusker, L. B.; Baerlocher, C. In *International Tables for Crystallography, Vol H.*; Gilmore, C. J., Kaduk, J., Schenk, H., Eds.; Wiley, in press.
(27) Smeets, S.; Xie, D.; McCusker, L. B.; Baerlocher, C.; Zones, S. I.; Thompson, J. A.; Lacheen, H. S.; Huang, H.-M. *Chem. Mater.* **2014**, *26* (13), 3909−3913.
(28) Smeets, S.; Xie, D.; Baerlocher, C.; McCusker, L. B.; Wan, W.; Zou, X.; Zones, S. I. *Angew. Chem.* **2014**, *126*, 10566−10570.
(29) Smeets, S.; McCusker, L. B.; Baerlocher, C.; Xie, D.; Chen, C.-Y.; Zones, S. I. *J. Am. Chem. Soc.* **2015**, *137*, 2015−2020.
(30) Smeets, S.; Koch, L.; Mascello, N.; Sesseg, J.; Hernández-Rodríguez, M.; Mitchell, S.; Pérez-Ramírez, J. *CrystEngComm* **2015**, *17* (26), 4865−4870.
(31) Dejoie, C.; Martinetto, P.; Tamura, N.; Kunz, M.; Porcher, F.; Bordat, P.; Brown, R.; Dooryhée, E.; Anne, M.; McCusker, L. B. *J. Phys. Chem. C* **2014**, *118* (48), 28032−28042.
(32) Porcher, F.; Borissenko, E.; Souhassou, M.; Takata, M.; Kato, K.; Rodriguez-Carvajal, J.; Lecomte, C. *Acta Crystallogr., Sect. B: Struct. Sci.* **2008**, *64* (6), 713−724.
(33) Fyfe, C. A.; Lee, J. S. J.; Cranswick, L. M. D.; Swainson, I. *Microporous Mesoporous Mater.* **2008**, *112* (1−3), 299−307.
(34) Meilikhov, M.; Yusenko, K.; Fischer, R. A. *Dalton Trans.* **2010**, *39*, 10990−10999.
(35) Smeets, S.; Liu, L.; Dong, J.; McCusker, L. B. *Inorg. Chem.* **2015**, *54* (16), 7953−7958.
(36) Amarante, T. R.; Neves, P.; Gomes, A. C.; Nolasco, M. M.; Ribeiro-Claro, P.; Coelho, A. C.; Valente, A. A.; Paz, F. A. A.; Smeets, S.; McCusker, L. B.; Pillinger, M.; Goncalves, I. S. *Inorg. Chem.* **2014**, *53* (5), 2652−2665.
(37) Majano, G.; Martin, O.; Hammes, M.; Smeets, S.; Baerlocher, C.; Pérez-Ramírez, J. *Adv. Funct. Mater.* **2014**, *24* (25), 3837−3837.
(38) Chen, R.; Yao, J.; Gu, Q.; Smeets, S.; Baerlocher, C.; Gu, H.; Zhu, D.; Morris, W.; Yaghi, O. M.; Wang, H. *Chem. Commun.* **2013**, *49*, 9500−9502.
(39) Burton, A.; Elomari, S.; Chen, C.-Y.; Medrud, R. C.; Chan, I. Y.; Bull, L. M.; Kibby, C.; Harris, T. V.; Zones, S. I.; Vittoratos, E. S. *Chem. - Eur. J.* **2003**, *9* (23), 5737−5748.
(40) Wu, M. G.; Deem, M. W.; Elomari, S. A.; Medrud, R. C.; Zones, S. I.; Maesen, T.; Kibby, C.; Chen, C.-Y.; Chan, I. Y. *J. Phys. Chem. B* **2002**, *106* (2), 264−270.
(41) Burton, A.; Darton, R. J.; Davis, M. E.; Hwang, S.-J.; Morris, R. E.; Ogino, I.; Zones, S. I. *J. Phys. Chem. B* **2006**, *110* (11), 5273−5278.
(42) Elomari, S.; Burton, A.; Medrud, R. C.; Grosse-Kunstleve, R. *Microporous Mesoporous Mater.* **2009**, *118* (1−3), 325−333.
(43) Burton, A.; Elomari, S.; Medrud, R. C.; Chan, I. Y.; Chen, C.-Y.; Bull, L. M.; Vittoratos, E. S. *J. Am. Chem. Soc.* **2003**, *125* (6), 1633−1642.
(44) Burton, A.; Elomari, S. *Chem. Commun.* **2004**, 2618−2619.
(45) Bergamaschi, A.; Cervellino, A.; Dinapoli, R.; Gozzo, F.; Henrich, B.; Johnson, I.; Kraft, P.; Mozzanica, A.; Schmitt, B.; Shi, X. *J. Synchrotron Radiat.* **2010**, *17* (5), 653−668.
(46) Baerlocher, C.; Hepp, A.; Meier, W. M. *DLS-76*; 1976.
(47) Coelho, A. A. *TOPAS-ACADEMIC*, v. 5.0; 2012.
(48) Momma, K.; Izumi, F. *J. Appl. Crystallogr.* **2011**, *44* (6), 1272−1276.
(49) Pettersen, E. F.; Goddard, T. D.; Huang, C. C.; Couch, G. S.; Greenblatt, D. M.; Meng, E. C.; Ferrin, T. E. *J. Comput. Chem.* **2004**, *25* (13), 1605−1612.
(50) Allen, F. H. *Acta Crystallogr., Sect. B: Struct. Sci.* **2002**, *58*, 380−388.
(51) Hanson, R. M. *J. Appl. Crystallogr.* **2010**, *43* (5), 1250−1260.
(52) Hanwell, M. D.; Curtis, D. E.; Lonie, D. C.; Vandermeersch, T.; Zurek, E.; Hutchison, G. R. *J. Cheminf.* **2012**, *4*, 17−17.
(53) Stephens, P. W. *J. Appl. Crystallogr.* **1999**, *32* (2), 281−289.
(54) Spek, A. L. *J. Appl. Crystallogr.* **2003**, *36* (1), 7−13.
(55) Zicovich-Wilson, C. M.; Gándara, F.; Monge, A.; Camblor, M. A. *J. Am. Chem. Soc.* **2010**, *132* (10), 3461−3471.

DOI: 10.1021/jacs.6b02953
J. Am. Chem. Soc. XXXX, XXX, XXX−XXX